Dynamic Frequency Support for Low Inertia Power Systems by Renewable Energy Hub with Fast Active Power Regulation

Nidarshan Kumar[1], Elyas Rakhshani[1], Zameer Ahmad[1], Jose Rueda Torres[1,*], Ebrahim Adabi[1], Peter Palensky[1], and Mart van der Meijden[1,2]

[1] Dept. of Elec. Sust. Energy, Delft University of Technology, Mekelweg 4, 2628 CD, Delft, The Netherlands
[2] TenneT TSO B.V., Arnhem 6812AR, The Netherlands
* Correspondence: j.l.ruedatorres@tudelft.nl,

Abstract: This paper overviews the application of Fast Active Power Regulation (FAPR) for different source of energies in a Renewable-energy hub system. In this study, FAPR strategies for frequency support is applied to various renewable resources like solar PV farm, a Type-4 full converter-based Wind Turbine and an Electrolyser acting as a responsive load. The power ratings of these renewable resources are based on a test system of a futuristic representation of the Northern of the Netherlands. The real-time EMT based simulations were performed to check the boundaries of operation of FAPR controllers and practical feasibility on the future power grid. The results prove that the control strategies and proposed topology can successfully provide frequency ancillary service by providing instant support to the grid during large frequency variations.

1. Introduction

Due Frequency is a steady parameter which is fixed constant to 50/60Hz at all voltage levels, be it generation, transmission or distribution levels. But when the grid is subjected to contingencies like loss of transmission, increase in load, forced generation outages or other load-generation imbalance events, the frequency becomes unstable. So, this instability affects various components starting from generators, transformers, and loads. Since the generation sources decide the system frequency, at generation level, there may be issues with load sharing. Also, due to multiple feedback loops operating at different time constants, issues of low-frequency harmonics, uncontrolled oscillations may lead to instability. Further, if the disturbances are sudden, torsional dynamics may cause rotor pole slip which can lead to large changes in currents which may activate the trip command [1]-[3].

During steady-state operation, in a power grid, there exists always a balance between generation and demand including losses. Now when a load-generation mismatch event occurs, the grid restoration to normalcy will be crucial and various generator auxiliary controllers enact, but since these controllers involve valve operation, they consume more time to enact. However, since synchronous generators within oil, coal, gas and nuclear plants run by large heavy rotating turbo-generators usually at 3000 RPM or 3600 RPM. The rotational kinetic energy involved will be huge which replicates to be the inertia of these generators in electrical terms. This forms the main backbone for immediate frequency regulation of 50Hz/60Hz under disturbance. Inertia is defined as a physical property of synchronous units which provides an inherent response to slow the Rate-of-Change-of Frequency (RoCoF). But in case of a low inertia power system with high share of power electronic converters and low share of synchronous generators, the concept of inertial support will be critical and hence the role of virtual inertia with advanced control-

Since most of the established renewable sources are Power Electronic Interfaced components with grid following configuration, the grid side Voltage Source Converters (VSC) injects the voltages and currents at a frequency as required at the point-of-common-coupling (PCC). Hence there is no mechanical power backing up the frequency, except in Hydro Energy [4]-[5]. Solar Photo-Voltaic (PV) is a classic example where the priority is to generate the most active power possible based on MPPT [8] and since it does not involve any rotating part and the power generated is primarily DC, and inertia emulation is possible only under power curtailed operation. Wind Energy has evolved over the years and now Type-4 Wind Turbines are the most common and established in the market which involves a complete back-to-back converter which isolates the generator and turbine from the rest of the grid, in order to shield the wind turbine setup from grid-related faults and to eliminate gear-box. The disadvantage with this is that the natural inertia that could have been extracted from the Wind Turbine Setup (Blades and Generator) is now lost. Flywheel technology in conjecture with tidal and bio-gas is still an emerging technology which can provide natural inertia support [10]-[11] but it is not an immediate solution. To summarize, only the major sources of renewable energy, like in its purest form cannot provide inertia support. But with slight modifications and careful tuning, these sources can provide the grid with virtual inertial support.

In this paper, a FAPR strategy is proposed for a renewable energy hub system for suppressing the frequency stability problem in low inertia system. Also, FAPR control strategy is tested to be a more generic concept and implementable in all renewable energy sources with suitable modifications. The developed FAPR controllers were implemented in a Type-4 wind turbine, solar PV farm and an electrolyser. A coordinative analysis between these systems during frequency curtailment period was demonstrated with detailed simulation model. Later, FAPR controller's performance were analysed by creating a generation load miss-match event. The intention of this study is not only to show improvement in RoCoF and Nadir but to analyse the limitations, side-effects caused due to FAPR controllers and lastly to see till what threshold we can utilize these control scheme considering safety and security of both the RES and the power grid. So this study starts with the description of North of Netherlands Network (N3), followed by the modifications done in order to create a Renewable-Energy system. Later a brief explanation of how the renewable energy sources have been modified to include FAPR shall be briefed and finally, the results of the simulations will be provided.

2. 2. Description of Test Model of the North of Netherlands Network (N3)

The test model was built in RSCAD inspired upon strategies of the 10-year development plan (2020 - 2030) of TenneT B.V (Dutch TSO) [12]. In a hypothetical future scenario, the installation of a largescale electrolyser plant is assumed in this study in the northern Netherlands. This part of the network includes a large-scale generation center, the connection of large-scale offshore wind and submarine interconnections with Norway (NorNed) and Denmark (COBRAcable) at Eemshaven and Eemshaven Oudeschip substations. Eemshaven Oudeschip is also a suitable location for a future 300 MW electrolyser plant, as abundant renewable energy generated by the offshore wind farm can be converted into hydrogen gas. The electrolyser plant can also support the power system stability by participating in ancillary services. The modeled system covers the EHV networks of voltage levels 380 kV and 220 kV and the year 2030 is taken into account to create synthetic profiles of generation and demand. The system also features two 2250 MVA thermal power plants equipped with two synchronous generation units each. Additional collaborative renewable energy via the HVDC inter-connectors are shared with Denmark (COBRAcable) and, Norway (NorNed) both operated at the rated power transfer capacity of 700 MW. Apart from this, N3 network houses 3058 MW onshore wind energy and 600 MW of offshore wind energy (Gemini wind park) distributed around the area which further aggregates into their corresponding 380 kV substations.

The synchronous generators models illustrate dynamic behavior due to detailed steam turbine governors enabled with droop control, AVR (Automatic Voltage Regulators) and PSS (Power System Stabilizers). This supports dynamic control and the provision of ancillary services during disturbance and post-disturbance periods. Wind turbines were represented by generic models, which are available in the software. For this study, it is assumed that the HVDC inter-connectors did not participate in the regulation of the system. Also, the local demands were clustered and modelled as constant loads. Figure 1 represents the load flow results of a N3 network of scenario 2030 [12].

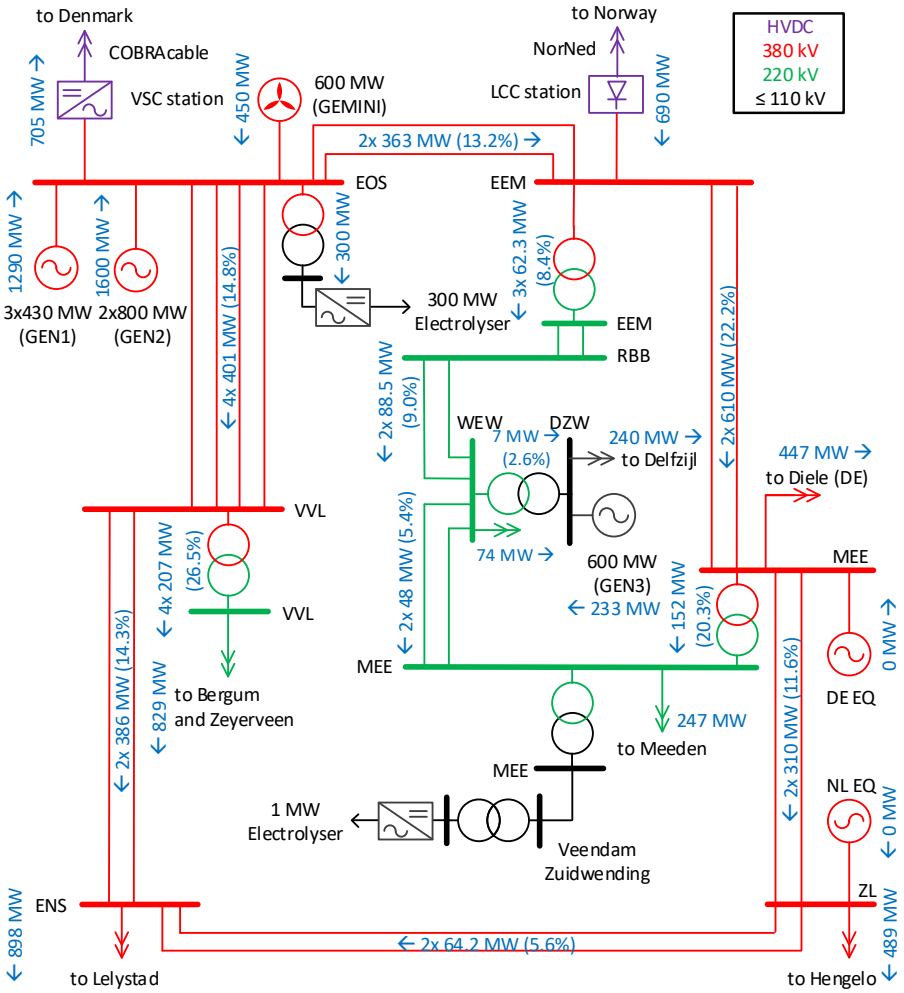

Figure 1. Power Flow for year 2030 of N3.

3 3. Modifications done in N3 Network to develop a Renewable-Energy System

In this paper, there are three main modifications done for frequency analysis. Firstly, an FAPR control strategy has been implemented in the electrolyser model in order to provide frequency ancillary support. Secondly, an 85MW full-scale Type-4 Wind Turbine has been implemented with integrated FAPR controllers. Thirdly, as shown in Figure 2, a solar farm of 300MW has been implemented with VSP based FAPR controller. The loads in the system have been adjusted accordingly. Here, the congestion in the grid has been increased mainly for 2 reasons. Firstly, to observe the effects of total system inertia reduction. Secondly to notice, if there are any other effects of congestion that could lead to system instability.

3.1 Frequency Regulation feasibility from a 300MW electrolyser model

Figure 3 Another component that was introduced in the N3 network was a 300MW Electrolyser as seen from the Figure 2. Here the electrolysers are used as regulatory, responsive loads which can vary their basic functionality of Hydrogen production as per available energy. Due to the in-deterministic behavior of power production observed from Wind and Solar, this concept which was earlier developed to maintain the security of supply in the power system by providing short-term balancing of renewable energy sources, is extended to a concept to regulate active power more instantly, so that frequency regulation is possible. Specifically, the stochastic behavior of these RES could be regulated by controlling the load of neighboring electrolysers to the probabilistic behavior of solar irradiance and wind speed.

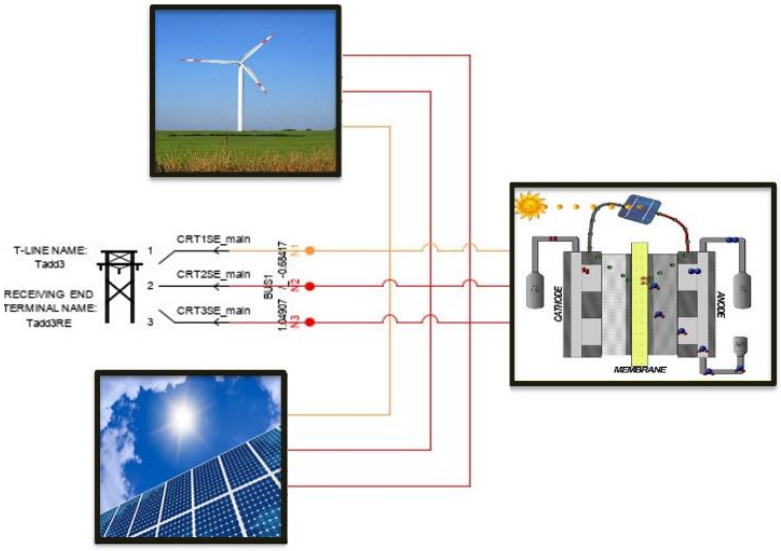

Figure 2. Screenshot of RSCAD implementation of Solar Farm, Wind Turbine Setup and Electrolyser.

In order to study the impact of a large-scale electrolyser in the Northern Netherlands Network, the 1 MW electrolyser model has been scaled up to a model of a 300 MW electrolyser plant. As shown in Figure 3, the model considered here is an aggregate model suitable for dynamic frequency analysis [13].

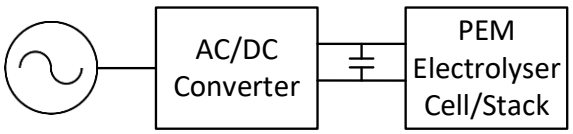

Figure 3. Block Diagram of the Inverter interfaced 300 MW electrolyser.

Although the electrolyser model shown in Figure 3 does not represent the real implementation of an electrolyser plant, this simplified model is sufficient for grid studies. Research is currently being continued to develop a model that accurately corresponds to the actual configuration of an electrolyser farm, which is a parallel connection of many smaller electrolyser stacks with each a capacity of several MWs. This model can provide more insight into the dynamics within an electrolyser plant. The main challenge of implementing this model in real-time simulations is, however, the limited capacity of the Real-Time Digital Simulator (RTDS).

3.2. Modified Solar Wind Farm with VSP based FAPR strategy

It is a fact that, since the solar power plants do not have a rotating mass, they cannot provide inertial support. But it is worth to note that, inertia can be emulated, synthetically,

from an additional battery source that can be connected to a stable DC link. Since the solar farm architecture provides a stable DC link and an inverter topology, VSP based FAPR controller could be implemented with suitable modifications. Figure 4 represents the connection diagram of a solar farm with VSP based FAPR controller.

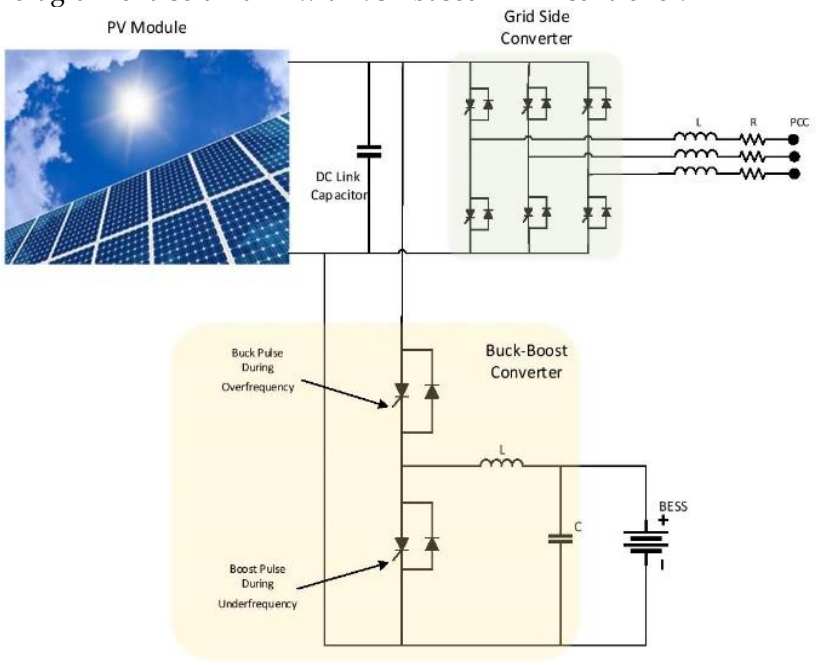

Figure 4. Architecture and connection diagram of a Solar Farm

For the case with Wind farm, a Type-4 wind turbine can be added in the same manner into an N3 system. It should be noted that the N3 network already had a Gemini Windfarm of 450MW. But this system was an average model which doesn't have a full-scale implementation and hence FAPR controllers couldn't be implemented. But in this case, full-scale type-4 wind turbine imposition served 2 purposes, mainly to display how the extraction of surplus inertial support can result in failure of Wind Turbines and another to prove the support of FAPR in a real N3 grid. As explained, the wind turbine blades' speed always settled to a lower value but never destabilized due to excess inertia extraction. This was due to DC link chopper protection, which regulated DC link voltage such that the WT always operates around MPPT and hence will not lose synchronism due to high energy extraction. But in this model, in order to check the inertia extraction limits, DC chopper has been disabled

$$P_{inertia} = \frac{KE_{rotor}}{\Delta t_{inertia}} = \frac{\frac{1}{2}J(\omega_{rotor}^2 - \omega_{rotor\_min}^2)}{\Delta t_{inertia}} \quad [W] \tag{1}$$

4. FAPR Definition and Control Strategies

FAPR constitutes a supplementary control acting on power electronic converters that link renewable generation, or storage, or controllable demand with an electrical power system. The input signal can be the measured system frequency and/or the deviation of active power. Next, a defined control structure dynamically adjust the the injection/absorption of active power in an attempt to quickly bound the frequency deviation resulting from a sudden active power imbalance. Frequency Stability studies in EMT based software of the FAPR Controllers are briefly presented in this section. FAPR controller can be one of the following three different controllers:

- Droop-based FAPR
- Droop-derivative based FAPR
- Virtual Synchronous Power based FAPR controller

The droop and the combined droop-derivative controller topology can be applied to RES which has a rotating mass that can expend some kinetic energy (ex. wind turbines) when needed, but VSP based topology is more suitable for any device which uses a full converter and has a stable DC link. Each of these controllers are evaluated in order to increase the penetration of PE interfaced generation of the grid without jeopardizing the security of supply in the power system.

4.1. Droop-Based FAPR

Frequency droop control is a control strategy which follows proportionality with a constant. The proportionality lies between input frequency error and the active power reference signal expected from the wind turbine during frequency curtailment period.

Figure 5 illustrates the droop control based FAPR controller. Here *F*meas represents the system frequency is measured. But since grid is large, the system frequency will be slightly different at different areas and hence inter-area oscillations exists, hence frequency at the most critical bus has been considered. The most critical bus is where the highest load frequency variation can be observed. Another input Fo equal to 50 Hz (in case of 50 Hz grid).

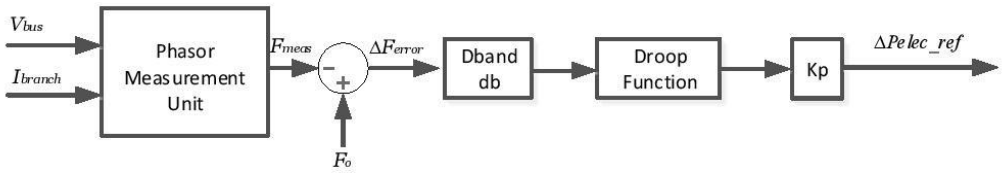

Figure 5. Droop-based FAPR

The error between the two input signals is passed through a dead band. From the grid codes [14], it was concluded that the frequency regulation controllers should be activated when deviation in frequency is beyond 0.06% to 0.1% from its nominal value. Based on this, the dead band can be between 0.03 to 0.05. In this case, dead-band was chosen to be 0.03 for the high sensitivity of the controller. This signal is further normalized using parameters based on IEC 61400-27 standards. The resulting signal is multiplied with a proportional or droop gain *K*p. The value of *K*p is truly system dependent. It is tuned based on the possible energy extraction from the wind turbine considering both grid side requirement and wind turbine side requirement. Grid side support being active, reactive power support while wind turbine side support includes expendable Kinetic Energy for safe operation considering wind forecasts. *P*elec-ref is the additional reference signal that is characteristically responsible for driving additional power from the PEIG.

4.2. Droop-derivative based FAPR

Figure 6 overviews the FAPR based on a droop-derivative FAPR. The set-point f_e and the frequency f and frequency deviation Δf determine the input of the controller. Δf is passed through two parallel control loops: The first one is a droop controller, which is described in the previous section. The actuation of the droop controller is active for the entire frequency curtailment period. The second loop is a derivative control, whose output is a derivative gain of the frequency error signal. The derivative controller is active only for the initial few seconds, and lasts until the frequency signal reaches the maximum allowed frequency deviation. The combined effect of the outputs of the droop-based loop and derivative-based loop produces ΔP_{elec_ref}, which modulates the active power response of the device(s) to improve both RoCoF and maximum frequency deviation (e.g. Nadir).

.

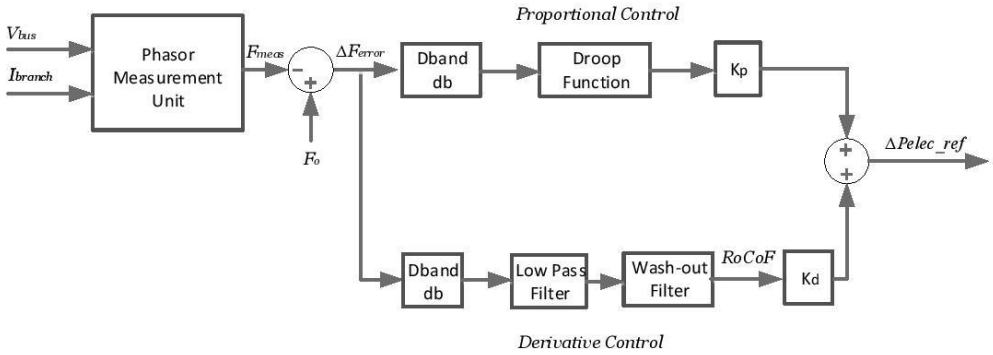

Figure 6. Droop-derivative based FAPR

The droop-derivative FAPR strategy should be tuned (taking into account system dependent dynamic properties) to cause a prominent ramping of the active power output at the AC side of a grid side converter, whenever an over/under-frequency event occurs.

4.3. Virtual Synchronous Power (VSP) based FAPR controller

The overall VSP setup has two parts namely battery power management system (BPMS) and VSP controller which is a signal generator.

A. Battery Power Management System

Figure 7 describes the block diagram of a BPMS which consists of a Bidirectional DC-DC converter, a Battery Energy Storage System (BESS) and at last the DC link of any VSC converter-based RES. A bidirectional DC-DC converter (shown in the Figure 7) is used to interface BESS to the DC link.

The main function is to appropriately discharge the battery as per the pulse generated from the VSP control block. VSP based FAPR control block is explained in detail in the next section. And depending on the power flow the bi-directional converter allows operation as a buck or a boost converter. They are individually controlled by two different signals. The control action of the converter is made in such a way that it allows controlled power flow in both directions

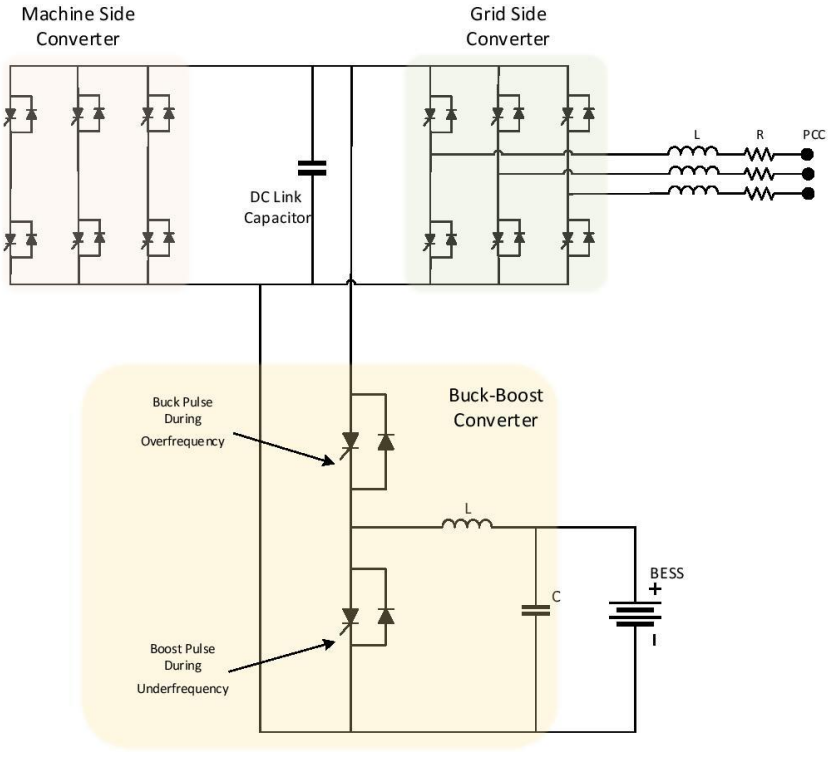

Figure 7. Block diagram of a VSP based battery power injection system.

B. VSP based Signal Generator

Figure 8 depicts the VSP controller, which measures the power required at the bus at the PCC to the reference power available at the bus. In this control scheme, ζ is the damping factor, ωn is the natural frequency for implementing this second-order function in RSCAD. Usually both these values will be equal during steady state condition, but during a load-frequency variation event, the measured power on the grid side deviates while the reference power that the RES delivers will remain same.

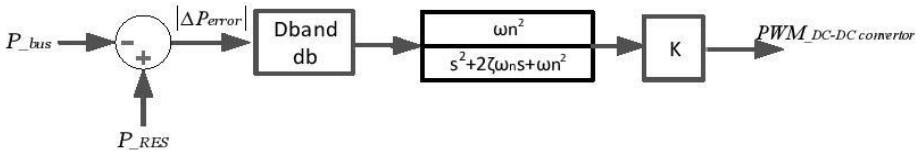

Figure 8. Block diagram of a VSP based FAPR controller.

This difference in power will result in error. For example, as shown in Figure 9, *P*_bus (Power going out from the Node bus) reacts to the grid when there is a load disturbance whereas *P*res will not. This difference will be taken as *P*error in the VSP control block which is further passed through a dead-band and later through a 2nd order transfer function mimicking a VSP topology. The details of the topology will be explained in the following section. The output of this block will be setting the duty cycle of a PWM controller. Hence the limits of this block shall be between 0 and 0.9. Based on the signal being sent to buck or boost converter, the switches are operated, and power will be withdrawn or injected into the DC link of RES respectively.

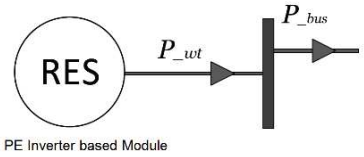

Figure 9. Connection of a Wind Turbine to the Power grid to indicate the inputs for VSP based FAPR controller

5. Simulation Results and Comparative assessment

The simulations tests, for N3 network with the generation data presented in Table 1, are performed in the following order, where only support from the electrolyser is first explored. In this case, FAPR controllers are implemented and tested against a load frequency event. Next, a solar farm of 300MW is connected to the network, at last, a Type-4 Wind turbine of 80MW is connected. The loads are increased accordingly. As discussed before, the synchronous generators are not replaced in this case due to the increase in renewables, just to observe the effect of a decrease in total inertia due to the share of renewable sources.

Table 1. Generation sources and imported power sources in the N3 for 2030 scenario

Generator/HVDC Link	Year 2030 Scenario
GEMINI Wind farm (EOS)	450 MW
NorNed Connection (EEM)	700 MW

COBRAcable Connection (EOS)	-700 MW
GEN1 (EOS)	3 × 430 MW
GEN2 (EOS)	2 × 430 MW
GEN3 (EOS)	233 MW
Total	**3490 MW**

To examine the response of electrolysers to frequency support, a generation load imbalance event was created, that is, a 200MW sudden loss of Gemini wind generation capacity is simulated. Due to this sudden loss in generation, there was an under-frequency event. Hence, the test on how the renewable sources can support this event through dispatch of frequency ancillary services will be discussed in the next subsections.

5.1. Frequency support through FAPR controllers implemented in Electrolysers

Electrolyser models which were present in the N3 network has been modified with the inclusion of droop, combined droop-derivative and VSP-based controller. So, during a load frequency event, the generation reduces and since electrolyser is a load, the FAPR controllers reduce the active power absorption accordingly, which will improve the frequency. Figure 10 represents the active power variation of the electrolyser and figure 11 depicts the resulting frequency improvement due to each controller. As observed from the base plot, the electrolyser on its own does not regulate its power demand under load-frequency event, but with the droop-based FAPR, taking into account the frequency deviation, the power demand of electrolyser was reduced which resulted in an improvement of Nadir. On the other hand, the droop-derivative FAPR helps in achieving a faster active power reduction. This improves RoCoF significantly, and also, as a by-product, even an improvement of Nadir is observed. The last controller which was implemented was VSP based FAPR controller, here, the VSP method is not integrated with the Battery Power Management System (BPMS), since electrolyser is a load and mostly the power regulation is by reducing the active power demand. The output of VSP is directly given to the active power reference input as in case of droop and combined droop-derivative controller. Also, please note that the droop controller is always active in combination with Derivative and VSP for the entire time. The time duration and active power reduction applied by derivative and VSP controller are different. VSP and derivative-based FAPR in application to Electrolyser is not different except how the inputs are measured and how the dynamics of error signal vary after the disturbance.

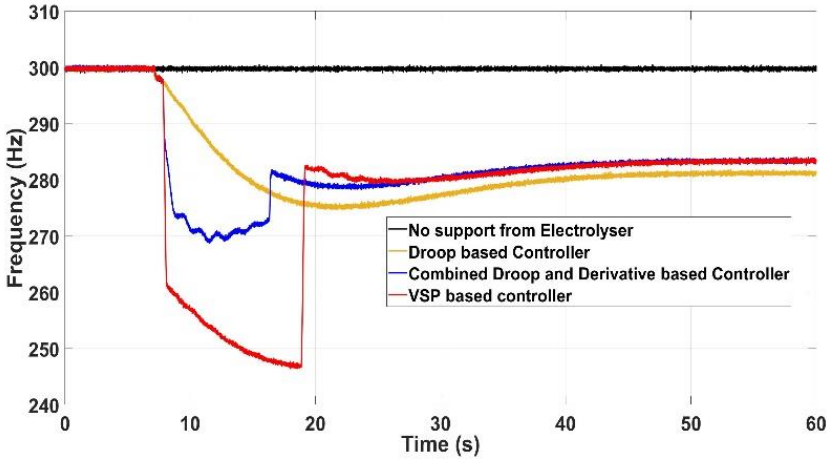

Figure 10. Shape of the power output due to the action of FAPR

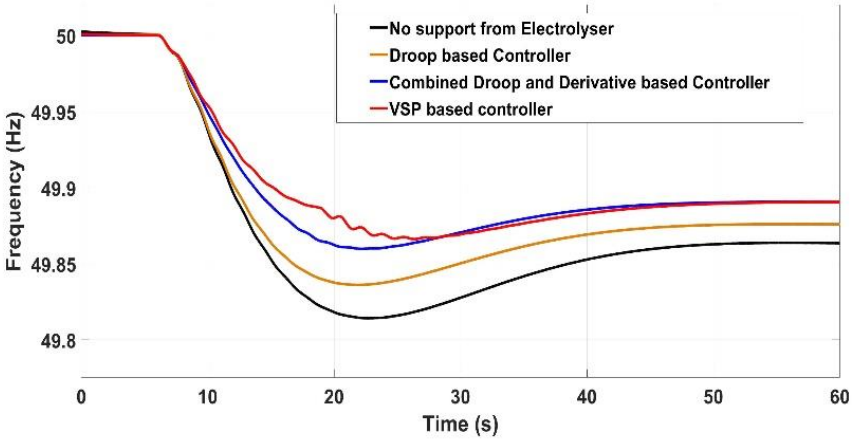

Figure 11. Shape of the frequency response due to the action of FAPR

5.2. Frequency support through VSP based FAPR controller implemented in Solar Farm

As explained before in section 5, a 300MW solar farm integrated and VSP based FAPR with BPMS has been implemented. Now with a 200MW sudden loss of Gemini wind generation capacity, the generation load mismatch event is simulated and solar farm under this event detects the event and provides support of 10% increase in active power i.e. 30MW for 10 seconds. As explained before more support in terms of higher active power injection and time of operation is limited by the size of BESS and grid side converter capabilities. Figure 12 depicts the improvement in frequency due to this inclusion.

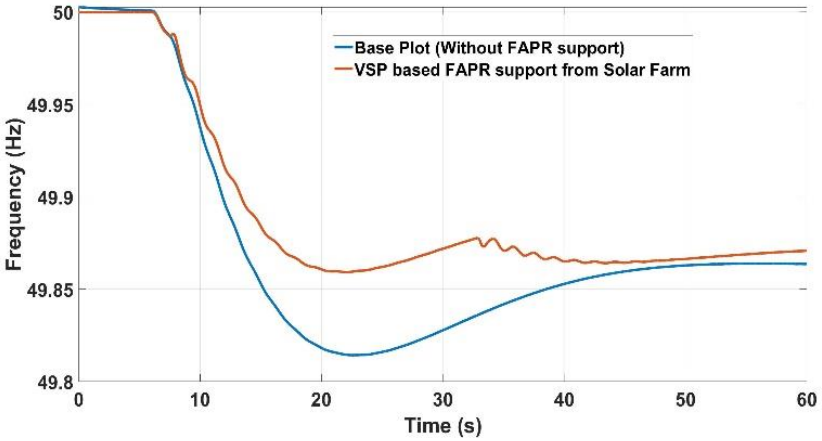

Figure 12. Frequency support from VSP based Solar Farm

It should be noted that higher the support in active power during the frequency containment period, higher will be the frequency improvement. This is regardless of any inverter interfaced renewable source.

5.3. Comparative assessment of RES integrated FAPR controllers

It is now evident that, if more RES are able to respond positively towards variation in system active power, by balancing out the effect by quickly altering their active power respectively, the frequency dynamics such as RoCoF and Nadir will improve. But also, the downside of sudden injection of active power in a low inertia system should be considered. To illustrate this effect, the VSP controller in the solar farm is suddenly activated sensing the frequency change, thereby giving 30MW of instant injection into the system. By comparing various plots in figure 13, it can be seen that the more RES sudden

regulations, the more crooked the frequency curve. And this effect becomes cumulative if the system inertia is low and may possibly disrupt the expected frequency dynamics as seen in fig 13.

A. Non-uniform or crooked frequency waveform

A comparative assessment between the various plots in figure 13 shows that the unevenness in the frequency waveform increases with increase in RES. This is because rotor swings of synchronous generators become predominant with lower system inertia [16]. Earlier the total system inertia was high since all the load demands were satisfied by purely synchronous generators but with the inclusion of RES and appropriate increase in loads, we see that the overall H/MW (inertia constant) in the system has reduced. This makes the synchronous generators more responsive if the disturbance event is close to them. A more detailed analysis has been shown in the next section.

B. Impact of Rotor Angle Swings and Inertia Response

In this section, the reason for the initial non-uniform frequency curve is analyzed more in detail. Also, with the load frequency variation concept understood, it is now possible to analyze the comeback of power system to a frequency deviation caused. The response can be divided into 4 stages:

Stage I: Generator Rotor Swings (first few seconds)
Stage II: Drop in Frequency (a few seconds to several seconds)
Stage III: Primary frequency control by the turbine governors (several seconds)
Stage IV: Secondary frequency control by the central regulators (several seconds to a minute).

Only the stages I and II are given importance in this study. As seen from the figure 1, the EOS bus is connected with 3x430MW and 2x800MW synchronous generators, a 300MW Electrolyser, a 700MW cobra cable load, 450MW Gemini Wind Farm. Now with a power imbalance of 200MW, there are 2 effects due to synchronous generators.

• The equivalent reactance of the system increases (generators are connected to each other in parallel), this reduces the amplitude of power angle characteristics.

• Secondly, the mechanical power delivered to the generators from the turbine will be low compared to the electrical demand, this decelerates the rotor and consequently, loss in kinetic energy. Later they follow the dynamics of equal area criterion to settle to normalcy. From the equation 2, with a fixed transient reactance value for a particular generator (higher the better for stability), the power swing deviates due to disturbance each generator's change its power angle and results in a swing before reaching steady-state.

$$P(\delta_0) = \frac{E'V_s}{x'_d} sin\delta' \quad (2)$$

$\delta 0$ = Initial Rotor Angle; x'd = Transient Reactance; E' = Instantaneous generator voltage; Vs = Voltage at the PCC.

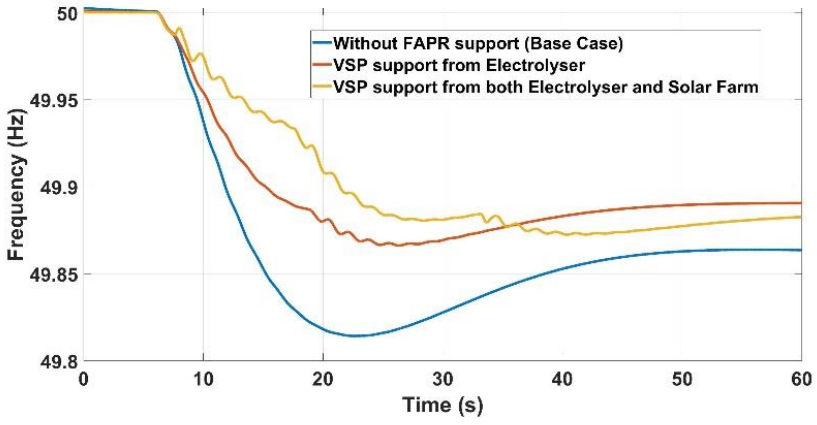

Figure 13. Frequency Comparison plots in a Renewable-Energy System Conclusions

Since this study aimed at proving FAPR controllers as a generic concept, they were implemented in Solar Farm and Electrolyser. So, with inertial response not possible through Solar Farm, only VSP based FAPR has been implemented and mitigation of frequency discrepancies have been demonstrated in section 5.2. Also, in section 5.1 a responsive load (electrolyser) is modified to support underfrequency event by quickly lowering is active power absorption, so that generation-load imbalance is reduced and frequency Nadir and RoCoF improved has been demonstrated. Here an important observation is that since electrolyser works on reducing its power output, it can support for all 3 stages (inertial, primary and secondary) of frequency regulation. Lastly, with the help of dynamic simulation tool, efforts have been made to explain Nadir and RoCoF behaviour with larger share of renewable energy. It is observed that with decrease in Inertia, the effect of non-uniformness is observed on local frequency curve which is dominated by the rotor angle swings of the nearest synchronous generators.

Nomenclature

RoCoF	Rate of Change of Frequency
BPMS	Battery Power Management System
BESS	Battery Energy Storage System
AGC	Automatic Generation Control

References

1. Power system stability and control. P Kundur. McGraw-hill, 1994.
2. E. Rakhshani, D Gusain, V Sewdien, JR Torres, M van der Meijden, A Key Performance Indicator to Assess the Frequency Stability of Wind Generation Dominated Power System, IEEE Access, Vol 7, 2019.
3. E. Rakhshani, Intelligent linear-quadratic optimal output feedback regulator for a deregulated automatic generation control system, Electric Power Components and Systems 40 (5), 513-533

4. E Rakhshani, H Mehrjerdi, A Iqbal, Hybrid wind-diesel-battery system planning considering multiple different wind turbine technologies installation, Journal of Cleaner Production 247, 119654
5. E Rakhshani, K Rouzbehi, A J Sánchez, AC Tobar, E Pouresmaeil, Integration of Large Scale PV-Based Generation into Power Systems: A Survey, Energies 12 (8), 1425, 2019.
6. E Rakhshani,Intelligent linear-quadratic optimal output feedback regulator for a deregulated automatic generation control system, Electric Power Components and Systems 40 (5), 513-533, 2012.
7. E Rakhshani, D Remon, P Rodriguez, Effects of PLL and frequency measurements on LFC problem in multi-area HVDC interconnected systems, International Journal of Electrical Power & Energy Systems 81, 140-152, 2016.
8. F. Low, I. Power, S. Using, and C. Technique, Primary Frequency Response Enhancement for Future Low Inertia Power Systems Using Hybrid Control Technique, (2018), 10.3390/en11040699.
9. M. Dreidy, H. Mokhlis, and S. Mekhilef, Inertia response and frequency control techniques for renewable energy sources : A review, Renewable and Sustainable Energy Reviews 69, 144 (2017).
10. J. I. Itoh, D. Sato, T. Nagano, K. Tanaka, N. Yamada, and K. Kato, Development of high efficiency flywheel energy storage system for power load-leveling, in INTELEC, International Telecommunications Energy Conference (Proceedings) (2014).
11. D. Curtiss, P. Mongeau, and R. Puterbaugh, Advanced composite flywheel structural design for a pulsed disk alternator, IEEE Transactions on Magnetics 31, 26 (1995).
12. Voor u ligt de Visie2030, een langetermijnvisie van TenneT op het 380 kV en 220kV deel van het landelijke elektriciteitstransportnet. (2017).
13. V. Ruuskanen, J. Koponen, K. Huoman, A. Kosonen, M. Niemelä, and J. Ahola, PEM water electrolyzer model for a power-hardware-in-loop simulator, International Journal of Hydrogen Energy, (2017).
14. E. Analysis, E. I. Division, and L. Berkeley, Review of International Grid Codes, (2018).
15. E. Rakhshani and P. Rodriguez, Inertia emulation in ac/dc interconnected power systems using derivative technique considering frequency measurement effects, IEEE Transactions on Power Systems 32, 3338 (2016).
16. J. Yan, C. Liu and U. Vaidya, "PMU-Based Monitoring of Rotor Angle Dynamics," in IEEE Transactions on Power Systems, vol. 26, no. 4, pp. 2125-2133, Nov. 2011, doi: 10.1109/TPWRS.2011.2111465.